



This is a repository copy of *Electrical properties and oxygen stoichiometry of Ba_{1-x}Sr_xTiO_{3-δ} ceramics*.

White Rose Research Online URL for this paper:

<https://eprints.whiterose.ac.uk/126250/>

Version: Accepted Version

Article:

Guo, M., Masó, N. orcid.org/0000-0003-0792-3943, Liu, Y. et al. (1 more author) (2018) Electrical properties and oxygen stoichiometry of Ba_{1-x}Sr_xTiO_{3-δ} ceramics. *Inorganic Chemistry*, 57 (1). pp. 64-71. ISSN 0020-1669

<https://doi.org/10.1021/acs.inorgchem.7b01827>

This document is the Accepted Manuscript version of a Published Work that appeared in final form in *Inorganic Chemistry*, copyright © American Chemical Society after peer review and technical editing by the publisher. To access the final edited and published work see <https://doi.org/10.1021/acs.inorgchem.7b01827>.

Reuse

Items deposited in White Rose Research Online are protected by copyright, with all rights reserved unless indicated otherwise. They may be downloaded and/or printed for private study, or other acts as permitted by national copyright laws. The publisher or other rights holders may allow further reproduction and re-use of the full text version. This is indicated by the licence information on the White Rose Research Online record for the item.

Takedown

If you consider content in White Rose Research Online to be in breach of UK law, please notify us by emailing eprints@whiterose.ac.uk including the URL of the record and the reason for the withdrawal request.



eprints@whiterose.ac.uk
<https://eprints.whiterose.ac.uk/>

Electrical properties and oxygen stoichiometry of $\text{Ba}_{1-x}\text{Sr}_x\text{TiO}_{3-\delta}$ ceramics

Mei Guo^{1,2}, Nahum Masó², Yang Liu² and Anthony R. West^{2,*}

¹Shandong University of Science and Technology, College of Electrical Engineering and Automation, Qingdao 266590, P. R. China

²University of Sheffield, Department of Material Science and Engineering, Mappin Street, Sheffield, S1 3JD, UK.

*E-mail: a.r.west@sheffield.ac.uk

Abstract

Ba_{1-x}Sr_xTiO₃ solid solutions prepared by solid state reaction in air at 1200-1400 °C, followed by slow cool to room temperature at the end of reaction, were essentially oxygen-stoichiometric and p-type. Their conductivity increased reversibly when either pO₂ in the surrounding atmosphere was increased or a dc bias as small as 1V was applied across the samples. The enhanced p-type conductivity is attributed to creation of mobile holes on under-bonded oxide ions. The same samples quenched from >~1400 °C were increasingly oxygen-deficient and n-type. They showed reduced conductivity with either a dc bias or increased pO₂, attributed to the trapping of mobile electrons. These materials provide a rare example of a switch between n-type and p-type conductivity, in the same material, linked to oxygen stoichiometry variation. In both n- and p-type materials, the samples responded to external stimulus in a similar way to a leaky capacitor; polarisation processes at sample surfaces led to first, charge storage and second, reversible change in bulk electrical properties.

Introduction

Both BaTiO₃, BT, and SrTiO₃, ST, have been the subject of very many studies for their intrinsic scientific interest and varied practical applications. Solid solutions between BT and ST show a smooth change in structure and properties, such as the ferroelectric Curie temperature which decreases with increasing Sr content¹⁻⁵. The electrical properties of BT are, however, very sensitive to both processing conditions and doping.

Oxygen loss from BT occurs at high temperatures and in atmospheres of low oxygen partial pressure, pO_2 , giving oxygen-deficient materials with n -type conductivity. Recently, it was shown that application of a small dc bias modified the electrical properties of doped BT⁶⁻¹⁵: acceptor-doped BT was p -type and showed increased conductivity⁶⁻⁸, whereas Mn-doped BT was n -type and showed decreased conductivity with an applied bias, as also did donor-doped rutile^{12,13}. Bias-dependent phenomena are of much current interest for memristive applications which are usually focused on thin film devices, whereas the above effects⁶⁻¹⁵ are reported in bulk materials. Two additional examples of unexpected, low-field changes in bulk properties are the reversible resistive switching at room temperature of Ca-doped BiFeO₃ ceramics¹⁴ and the low field introduction of electronic conduction into oxide ion-conducting yttria-stabilised zirconia, YSZ¹⁵.

It has been reported that BST solid solutions show a p - to n - transition at 1400 °C¹⁶; it was of interest to investigate this further, to determine the effect of possible oxygen non-stoichiometry on the transition, depending on sample processing conditions and to understand better the origin of the p -type behaviour. The results are reported here. A new model for the effects of either dc bias or changing pO_2 on the electrical properties, which treats the sample as a leaky capacitor is proposed.

Experimental

Samples of $\text{Ba}_{1-x}\text{Sr}_x\text{TiO}_3$, BST ($x = 0.2, 0.3, 0.4, 0.5, 1.0$) were prepared by solid state reaction using BaCO_3 (Aldrich 99%), TiO_2 (Aldrich 99.9%) and SrCO_3 (Aldrich 99%), which were dried prior to weighing at 180 °C, 800 °C and 180 °C, respectively. Samples totalling ca. 3g were mixed with acetone manually in a mortar and pestle, dried and fired in Pt crucibles, initially overnight at 1050 °C to decarbonate the BaCO_3 and initiate reaction, followed by 1100 °C for two days in air with daily regrinding. Pellets were prepared by uniaxial pressing. Pellets of $x = 0.2$ were heated in air at one of three temperatures: 1200, 1300, 1400 °C, each for 6 h and cooled slowly inside the furnace. It was found that the permittivity results were improved for pellets heated at 1400 °C, and therefore, pellets of $x = 0.3, 0.4, 0.5, 1.0$ for permittivity measurements were also heated in air at 1400 °C for 6 h and cooled slowly inside the furnace.

It was also found that the conductivity of pellets depended on both the final heating temperature and subsequent cooling rate. This was because samples lost a small amount of oxygen at high temperatures which was at least partly recoverable on cooling. To quantify the effects of oxygen loss, a selection of pellets, wrapped in Pt foil envelopes, was reheated at different temperatures in a vertical tube furnace and, at the end of the heat treatment, quenched by dropping into liquid N_2 ; cooling rates were estimated to be $\sim 250 \text{ °C sec}^{-1}$.

The phases present were analysed by X-ray Powder Diffraction, XRD, using a Stoe Stadi P Diffractometer (Darmstadt, Germany), $\text{CuK}\alpha_1$ radiation, with linear position-sensitive detector. The tetragonal and cubic lattice parameters were determined from XRD data by least-squares refinement for reflections in the range $20 < 2\theta < 80^\circ$, using the software WinXPow, version 1.06.

For the pellets of $x = 0.2$, electrodes were fabricated on opposite pellet faces from either Au, Pt or Ag paste, which was dried and decomposed by gradually heating to 800 °C for 2 h, 900 °C for 1 h and 600 °C for 1 h, respectively. Similarly, for pellets of $x = 0.3, 0.4, 0.5, 1.0$, electrodes were

fabricated on opposite faces from Au paste. In order to measure the electrical properties of quenched samples, sputtered Au electrodes were attached after the final high temperature quench. Samples with electrodes attached were placed into a conductivity jig and measured either at fixed frequencies over the temperature range -60 to 250 °C using an LCR meter or using an Agilent 4294A impedance analyser over the frequency range 40 Hz to 10 MHz and temperature range, room temperature to 800 °C. Impedance data were corrected for overall pellet geometry and for the blank cell capacitance (jig correction). Resistances are given in units of Ω cm, which correspond approximately to resistivities of the sample bulk, but not of grain boundaries since these were not corrected for grain boundary geometry.

Results

Samples of $x = 0.2$ appeared to be single phase by XRD after firing at 1200 , 1300 and 1400 °C and the data closely resembled those of tetragonal BT. For $x = 0.3$, 0.4 , 0.5 , 1.0 , the samples also appeared to be single phase but were cubic. XRD patterns were indexed accordingly; refined lattice parameters, **Fig. S1** show a linear decrease with x , consistent with literature data^{1,2} that also show a tetragonal to cubic change in the range $x = \sim 0.2$ – 0.3 .

In order to make a preliminary survey of the electrical properties and assess the homogeneity of the BST solid solutions, fixed frequency, 100 kHz, sweeps of the permittivity were made as a function of temperature; results for one composition, $x = 0.2$, sintered at three temperatures are shown in **Fig. S2**. For ceramics sintered at 1200 °C, the permittivity maximum associated with the ferroelectric–paraelectric Curie temperature was broad, indicating either small particle size, variation in crystallinity, or compositional inhomogeneity. Samples sintered at 1400 °C showed a much sharper permittivity maximum, with $T_c \sim 65$ °C for $x = 0.2$, that is 62 °C lower than T_c for

undoped BT, 127 °C.

Fig. 1(a) shows the permittivity at 100 kHz of samples $x = 0.2\text{--}0.5$ sintered at 1400 °C and corresponding Curie-Weiss plots, **Fig. 1(b)**; T_c and T_o values extracted from the peak maximum temperatures are summarised in **Table S1**. T_c decreases linearly by 3.4 °C per mol% Sr, consistent with literature data³⁻⁵ and is direct evidence that Sr^{2+} ions enter the BT lattice.

Fig. S3 shows fixed frequency sweeps of $\tan \delta$ for $x = 0.2$ sintered at 1200–1400 °C; losses in the region of T_c are similar, *e.g.* ~ 0.05 at 10 kHz, but less temperature-sensitive for the sample sintered at 1200 °C and are attributed to increased polarization phenomena in the region of T_c . Samples became increasingly lossy above 150–200 °C, especially for the sample sintered at 1200 °C which is attributed to the increase in electronic conduction at higher temperatures.

In order to better characterize the effect of processing conditions on electrical microstructures and properties, impedance measurements over the range 40 to 10^7 Hz were carried out for a range of temperatures. Presentation and analysis of a typical set of impedance complex plane, Z^* , plots at two temperatures, **Fig. 2(a,b)**, showed two main resistances, attributed to the bulk resistance, R_1 and grain boundary resistance, R_2 which together, dominated the total resistance, $(R_1 + R_2)$. The same data, for these and other temperatures, presented as spectroscopic plots of capacitance, C' , **Fig. 2(c)**, demonstrated a frequency-independent, but temperature-dependent plateau at high frequencies attributed to the sample bulk capacitance, C_1 . Its value, *e.g.* $3 \times 10^{-11} \text{ Fcm}^{-1}$ at 500 °C, decreased with increasing temperature and is characteristic of a ferroelectric material above T_c ; the data shown at 51 °C were obtained just below T_c . A second plateau in C' at lower frequency with value $\sim (3\text{--}4) \times 10^{-9} \text{ Fcm}^{-1}$ is seen at higher temperatures (c) and is attributed mainly to a conventional grain boundary capacitance, C_2 .

The possible effect of electrodes on electrical properties was tested by using electrodes of Au, Pt

and Ag on sample $x = 0.2$. All datasets showed a similar impedance response to that in **Fig. 2**; values of R_1 and R_2 are presented as Arrhenius plots of $\log \sigma$ vs T^{-1} in **Fig. 3(a)**. The activation energies and magnitudes of the conductivities were unaffected by the choice of electrode, demonstrating that the impedance data were sample-related and not associated with sample–electrode contacts, such as Schottky barrier formation.

Data for R_1 for a range of compositions are shown in **Fig. 3(b)**; all plots are either linear or have a small curvature and activation energies (which do not take account of any curvature) in the range 1.00 to 1.36 eV; there is no obvious variation in bulk conductivity with x .

Impedance data in atmospheres of different oxygen partial pressure, pO_2 , are shown in **Fig. 4** for two samples of $x = 0.2$ cooled from high temperature at very different rates, estimated approximately as $5\text{ }^\circ\text{C min}^{-1}$ (a) and $250\text{ }^\circ\text{C sec}^{-1}$ (b). For both, the sequence of measurements was first in N_2 , second in O_2 and third in air.

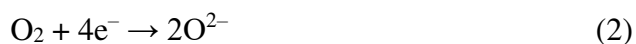
For the slow-cooled sample (a), both R_1 and R_2 at $550\text{ }^\circ\text{C}$ decreased with increasing pO_2 . A decrease in bulk / grain boundary resistance with increasing pO_2 is a characteristic of materials that are modest electronic conductors in which the main charge carriers are holes. In addition, the number of holes increased with pO_2 and must, therefore, be associated with the adsorption and subsequent ionisation of O_2 molecules at or near the sample surface, as represented by the simplified, ideal equation:



From these results, therefore, this heat treatment which concluded with a slow cool in air from $1400\text{ }^\circ\text{C}$, gave a sample that was both p -type and whose hole concentration was easily modified by changing pO_2 in the surrounding atmosphere.

By contrast, for a sample quenched in air from $1440\text{ }^\circ\text{C}$, **Fig 4(b)**, the conductivity decreased

with increasing pO_2 , indicating removal of charge carriers and therefore, n -type behaviour, eq'n (2):



These results are in agreement with literature data of conductivity *vs* pO_2 which show that the conduction mechanism in air changes from p -type to n -type above 1400 °C¹⁶.

The essential features of the oxygen adsorption / dissociation / ionisation reactions involved with eq'ns (1) and (2) are the same and both require the participation of electrons from the sample. The differences are that pre-existing n -type conduction electrons are involved in eq'n (2), whereas in eq'n (1), the electrons that lead to formation of the O^{2-} ions must arise from a secondary ionisation process. Usual explanations in the ceramic literature attribute the source of such electrons in p -type materials to the presence of unavoidable impurities such as Fe^{3+} which ionise to Fe^{4+} . An alternative possibility is that ionisation of underbonded O^{2-} ions is responsible for the electrons. The holes that are created remain on oxygen as O^- ions⁶⁻¹¹ and the resulting p -type conductivity is attributed to hopping of holes between adjacent oxygens; since the O^- ions are surrounded by lattice O^{2-} ions, there is always a three-dimensional conduction pathway available for hole conduction, which may not be the case if the holes were located on a small concentration of Fe^{3+} impurities. In support of the model with location of holes on underbonded oxide ions is the observation that pO_2 -dependent, p -type conduction occurs in a wide range of Ba-, Sr- and Ca-titanate perovskites that are acceptor-doped; by contrast, the electronic conductivity in donor-doped materials is usually n -type^{12,13}.

In order to study the effect of applied dc voltage on the ac electrical properties, impedance measurements were made at the same time as a small dc bias of 10 V was applied across the same two samples of $x = 0.2$, slow-cooled from 1400 °C and quenched from 1440 °C. For a pellet thickness of 2.2 mm, this voltage corresponded to a gradient of 46 Vcm^{-1} . For the slow-cooled

sample, impedance measurements at 400 °C, **Fig. 5**, varied with time: R_1 decreased gradually (b), before reaching a steady state after several hours. R_2 also decreased greatly with time, although its value was too large to be measured before applying the *dc* bias. Spectroscopic plots of admittance, Y' for the same data (c) showed that the total sample resistance, R_t , dominated by R_2 , decreased with time. This decrease in resistances observed with *dc* bias, as well as with increasing pO_2 , **Fig. 4(a)**, is an indication of *p*-type behaviour. On removal of the *dc* bias, the impedance data gradually returned to their original values (not shown).

The combined effects of pO_2 and a *dc* bias of 1, 5 and 10V for the sample slow-cooled from 1400 °C is shown at 600 °C in **Fig. 6**. The measurement temperature, 600 °C, was chosen for convenience since the resistance changes occurred much more rapidly than at lower temperatures; after each set of measurements, the *dc* bias was removed and the sample allowed to recover its original ground state before either the atmosphere was changed, or the bias increased, for the next set of measurements. The bulk conductivity increased on changing from N_2 to air to O_2 ; further, in each atmosphere, the conductivity increased with time on application of a *dc* bias during the impedance measurements before reaching a steady state; the value of the steady state conductivity also increased with bias.

For a sample of $x = 0.2$ quenched from 1440 °C, the combined effects of pO_2 and *dc* bias are seen by comparing **Fig 4(b)**, for the effect of pO_2 at 206 °C and **Fig 7** for the effect of 10 V *dc* bias on the same sample as a function of time, in air, at 197 °C. From this, it is concluded that, as both bulk and grain boundary resistances increased, they are both *n*-type.

Similar results (not shown) were obtained for composition $x = 0.5$: for samples quenched from high temperatures, both bulk and grain boundary resistances were *n*-type whereas samples that were either slow-cooled or quenched from lower temperatures were *p*-type. For samples quenched from

intermediate temperatures, the results were less clear-cut; in some cases, the bulk and grain boundary resistances in a particular sample behaved differently; in others, one or other of the resistances showed little variation with atmosphere or bias. It appears therefore, that materials quenched from intermediate temperatures were close to the cross-over between *p*- and *n*-type behaviour; there was no evidence of a significant region of pO_2 space in which the conductivities were independent of pO_2 . Although some oxide materials show an electrolytic domain associated with oxide ion conduction between *n*-type and *p*-type regions, there was no evidence in these samples of a significant amount of oxide ion conduction.

During the heat treatment of samples of composition $x = 0.2$, it was noticed that their colour depended on both temperature and cooling rate. Samples were typically white when quenched from 1400 °C, grey when quenched from 1430–1450 °C and black when quenched from 1470 °C, but white when slow-cooled from any temperature in the range 1400–1470 °C. The colour changes with increasing quench temperature were attributed to increasing oxygen loss; at each quench temperature, the oxygen stoichiometry of the samples was effectively frozen-in, but reversible uptake of oxygen occurred during slow cooling and caused a return to white colour. In order to quantify the amount of oxygen loss, a sample placed in a Pt envelope was sequentially quenched and slow-cooled from 1470 °C and weighed after each cool; this experiment was repeated three times. The results, **Table 1**, showed a consistent, small difference in mass between quenched and slow-cooled samples, from which, assuming that the slow-cooled sample was fully oxygen-stoichiometric, the stoichiometry of the quenched sample, and therefore, the stoichiometry, in air, at 1470 °C, was calculated to be $Ba_{0.8}Sr_{0.2}TiO_{2.9885}$. The mass differences were too small to be detected by standard thermogravimetry, which is why accurate mass measurements on 0.5 g-sized pellets that were successively quenched and slow-cooled were made.

The colour changes associated with variable oxygen stoichiometry are attributed to variable electron content of the Ti 3*d* orbitals of the BST perovskite structure, which is controlled by oxygen deficiency, δ in the general formula $\text{Ba}_{1-x}\text{Sr}_x\text{TiO}_{3-\delta}$. This is also demonstrated clearly by the conductivity of samples quenched from different temperatures, **Fig. 8**. Both compositions, $x = 0.2$ and 0.5 , showed a dramatic increase in conductivity and associated reduction in activation energy with increasing quench temperature in the range 1400–1470 °C. However, for both compositions, the conductivity of the sample quenched from 1400 °C was the smallest and increased somewhat either for the slow-cooled sample or for samples quenched from temperatures below 1400 °C. Clearly, a change in conduction mechanism occurred for samples quenched from above and below 1400 °C.

Discussion

We report here several sets of results which, collectively for BST solid solutions, offer considerable new insight into the high temperature oxygen non-stoichiometry, the magnitude of the electronic conductivity, the nature of the temperature-dependent *p-n* transition and the sensitivity of conductivity to both $p\text{O}_2$ and *dc* bias, as follows:

1. The BST solid solutions lose a small amount of oxygen at the high temperatures that are usually used in sample synthesis. The loss increases with temperature, at least over the range 1400–1470 °C and for instance, from the measurement of reversible weight changes of samples of $x = 0.2$ that were either quenched or slow-cooled, the oxygen stoichiometry was calculated to be $\text{Ba}_{0.8}\text{Sr}_{0.2}\text{TiO}_{2.9885}$ at 1470 °C. Assuming that equations (1) and (2) represent, ideally, the gas–solid equilibria involving oxygen exchange at sample surfaces, then the consequence of oxygen loss is that the samples liberate electrons, reverse of equation (2), which enter the crystal lattice. The only

sites in the BST lattice that can accept such electrons are the $3d$ orbitals on Ti. Partial occupancy of Ti $3d$ orbitals often leads to high conductivity and therefore, as in this case, evidence for oxygen loss is provided, clearly but indirectly, by an enhancement in n -type conductivity and a reduction in activation energy for conduction. This is shown for two compositions in **Fig. 8**: for both, large increases in conductivity and reduction in activation energy occur with increasing quench temperature. The variation in oxygen stoichiometry is close to the limit of what can be detected by careful weight loss measurements. It was quantified at one temperature, 1470 °C, but the results may depend on sample parameters such as grain size, porosity, surface area, time and furnace atmosphere.

Although oxygen loss at high temperatures is a common phenomenon, as observed in for example, pure BT, rutile TiO₂ and SnO₂,¹⁷⁻¹⁹ it is important to recognise that, in order to see the associated increase in conductivity, rapid cooling rates are essential to preserve the oxygen-deficiency to room temperature. With the typical cooling rates that are obtained for samples fired in box furnaces or horizontal tube furnaces and either programme-cooled inside the furnace or cooled more rapidly by removing from the furnace at temperature and allowing to cool in air, partial or complete oxidation may occur during the final cooling stage. Cooled samples may therefore be insulating and show little remaining evidence of the oxygen deficiency that had been present at high temperatures. They may, alternatively, develop a core-shell structure consisting of a conducting core and an insulating shell as a result of partial oxidation: slow oxygen diffusion rates can lead to an oxygen concentration gradient between the fully oxidized surface and oxygen deficient core.

To study the electrical microstructure and for instance, the presence of core-shell structures, the ac impedance technique is invaluable because each electrically-different region of a sample has its own time constant and can, in principle, be separated on a frequency scale. By contrast, dc

measurements give only the total sample impedance, which is dominated by the largest resistance, assuming that the component resistances are connected in series. The large difference in conductivity of slow-cooled and quenched samples, such as shown here and the variety of electrical microstructures that may be produced, demonstrates the critical influence on sample properties of the post-sinter cooling conditions. In our slow-cooled samples, there was no evidence of a core-shell structure and a residual conductive core; it appears, therefore, that the cooling rate was sufficiently slow to achieve samples that were fully oxygen-stoichiometric.

2. The effect on conductivity of pO_2 and dc bias was similar: either the conductivity decreased with both increasing pO_2 and dc bias, or it increased. The explanation of these effects is most straightforward for n -type materials since only one variable, the number of pre-existing charge carriers, is affected. With n -type materials, equation (2) is driven to the right with increasing pO_2 ; electrons are withdrawn from the sample, trapped by the formation of reduced oxygen species at the surface and the conductivity decreases. This is expected to occur equally at all sample surfaces exposed to the atmosphere and leads to a slight charge imbalance between sample surface and interior. The response of n -type materials to decreasing pO_2 leads to the opposite effect; reduced oxygen species are desorbed from the sample surface, the released electrons lead to an increase in charge carrier concentration in the sample interior and the conductivity increases.

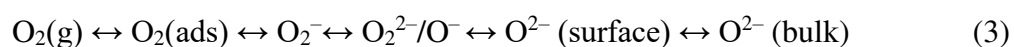
On application of a dc bias, electrons in n -type materials are attracted to the positive electrode and again, are trapped by the formation of reduced oxygen species at the sample surface, equation (2). At the negative electrode, the reverse process could in principle involve injection of electrons into the sample; this effect, if it occurs at all, would lead to an increase in n -type carrier concentration, thereby cancelling fully or partially the changes at the positive electrode. Under certain circumstances, charge injection from the negative electrode may occur, but it appears either

to be not important with the present materials and conditions or to not influence the dominant, bias-dependent change in sample conductivity caused by electron trapping at the positive electrode.

The response of *n*-type samples to either an increase in pO_2 or to a *dc* bias may be likened to the charging of a leaky capacitor: the exterior surface of the sample develops a small negative charge which is balanced by the positive charge created in the sample interior. Since mobile carriers are removed from the sample by this process, the sample interior becomes less leaky and its resistance increases. On removal of the bias, the capacitor discharges as electrons trapped at the surface are released and the conductivity returns to its original value as electron-hole recombination occurs.

On application of a *dc* bias to a *p*-type material, electrons are again attracted to the positive electrode but these electrons, and the associated holes, must be generated by a secondary ionisation process. Consequently, charge imbalance between sample surface and interior again results with trapped electrons at the sample surface and holes in the sample interior; in this case, however, holes are the principal charge carrier and the sample becomes more leaky due to the increase in *p*-type conduction. On removal of the bias, the changes are reversible and autodischarge occurs as electrons trapped at the surface recombine with holes in the sample interior.

Equations (1) and (2) are an oversimplification of the gas-solid equilibria involving oxygen species that must be active at the surface of ceramic oxides. Surface science studies show the presence of species such as superoxide and peroxide ions at the surfaces of many materials. Although we have no direct data for the present BST materials and their surfaces, the following equilibria are likely to be present at BST surfaces:



The various equilibria may be displaced to the right, by either increasing pO_2 or application of a positive bias, both of which involve (i) removal of electrons from the sample and (ii) increase in

concentration of reduced oxygen species at the sample surface. This accounts for the observation that application of a *dc* bias and an increase in pO_2 have qualitatively similar effects on sample conductivity.

3. In order to account for the changes in *p*-type conductivity, holes must be created. Since conduction is thermally-activated in the present materials, the holes must be located on specific atomic species. Traditionally, in nominally-insulating ceramic oxides, holes are presumed to be located on unavoidable impurities such as Fe that are either present in the starting materials or introduced during the various milling and firing procedures. However, the accumulated evidence on a range of high purity, *p*-type, acceptor-doped oxide ceramics points to the location of holes on oxygen since there are no cations present that can be readily ionised to a higher oxidation state. The oxygen-containing holes may therefore be regarded as O^- ions, although these are not usually considered to be probable species in bulk, stoichiometric oxide structures.

Two ways to generate O^- ions may be envisaged; both involve ionisation of *underbonded* O^{2-} ions, *i.e.* O^{2-} ions that are surrounded by an effective positive charge that is less than 2+. First, underbonded oxide ions may be associated with acceptor impurities or dopants that have lower charge than required by the host lattice. Examples are provided by BT that has Zn, Mg or Ca substituted for Ti at the 1 % level⁶⁻⁸. Thus, in a cubic perovskite such as $SrTiO_3$ with a cubic lattice parameter *c*, each oxygen is surrounded by 2 Ti at a distance $a/2$ and 4 Sr at a distance $a/2\sqrt{2}$. If either Ti or Sr is replaced by a cation of lower charge or indeed, one of the cation sites is vacant, then the amount of positive charge in the immediate vicinity of the oxide ion is reduced, which may therefore be regarded as underbonded.

Second, oxide ions at sample surfaces and interfaces may be coordinatively unsaturated; some structural reorganisation may occur compared with the lattice interior, but unless fully-covalent,

non-polar surface structures evolve, some degree of underbonding, of either cations or oxide ions, is likely.

In either case, O^{2-} ions that are underbonded are destabilised. This is because O^{2-} ions in the gas phase are spontaneously unstable. O^{2-} ions exist in crystal lattices only by virtue of (i) the surrounding positive charge which has a net effective value of 2+ in an electroneutral structure such as most oxides and (ii) the increased lattice energy arising from Coulombic interactions associated with structures made of divalent oxide ions compared with (hypothetical) structures based on monovalent oxide ions.

Depending on the degree of underbonding and therefore, their environment, O^{2-} ions may ionise:



This reaction can be driven to the right in a positive potential gradient or, alternatively, by surface adsorption and ionisation of oxygen molecules in reactions such as:



Depending on conditions, therefore, O^{-} ions and species such as superoxide, O_2^{-} species may be created, either by application of a *dc* bias, equation (4) or increasing pO_2 , equation (5). Although we have no direct evidence for superoxide formation in the present BST materials, evidence for superoxide formation and *p*-type conductivity was found in Ca-doped BT that had been re-oxidised after high temperature synthesis²⁰. In that case, the concentration of superoxide ions was controlled by the oxygen vacancy concentration in the host lattice whereas here, we consider the possibility that they may also form more generally at sample surfaces.

We can now see that one of the steps in the response of both *p*- and *n*-type materials to changing pO_2 and *dc* bias is the same and involves trapping of electrons at sample surfaces. This single step accounts for the behaviour of *n*-type materials. The overall response of *p*-type materials

is more complex and additionally requires the creation of holes. The only realistic possibility involves ionisation of underbonded oxide ions which may be driven, at least in part, by the trapping of electrons generated in the sample interior at the sample surface.

4. The switch from *n*-type to *p*-type conductivity of BST solid solutions with decreasing quench temperature, is envisaged to be as follows. For temperatures of 1430 °C and above, the conductivity is controlled by oxygen loss; associated electrons are the majority charge carriers and conduction is *n*-type:



At lower quench temperatures, oxygen non-stoichiometry is less and the materials are *p*-type. There are two possible origins of the holes that lead to *p*-type conduction.

First, at 1400 °C and below, the BST solid solutions are accurately oxygen-stoichiometric. Nevertheless, O₂ molecules are able to adsorb on sample surfaces and, by means of reaction 5 or similar reactions, O⁻ species are created which become the principal sources of the observed hole conduction. Such oxygen adsorption is favoured by slow cooling or annealing at lower temperatures and, as shown in **Fig 8**, the conductivity increases somewhat with a reduction in annealing temperature. The activation energy for *p*-type conduction is different from that for conduction of *n*-type samples quenched from above 1400 °C.

Second, the BST solid solutions which were prepared to be cation-stoichiometric may, in reality, have been slightly deficient in BaO/SrO due to reaction with the Pt crucible during high temperature firing. This may lead to Ba/Sr vacancies in the BST crystal structure and the effective doping with zero-valent acceptor ions. Previous studies have shown that BT samples which were prepared with a controlled deficiency of either Ba or Ti showed significant *p*-type behaviour, unlike samples which were cation stoichiometric. At present, we are unable to distinguish between these

two possible mechanisms of hole creation, but do note that the overall effect on the electrical properties is much less than associated with oxygen-deficient *n*-type conduction, **Fig 8**.

5. The bias- / pO_2 - dependent conductivity changes are time-dependent for both *p*-type, **Fig 6**, and *n*-type BST. The overall changes are also fully reversible. The rates are therefore controlled by either thermally-activated diffusion processes or ionisation/reformation of underbonded O^{2-} ions. The behaviour of *n*-type material is, in principle, more simple since diffusion of only one species, *n*-type electrons is involved. For *p*-type materials, diffusion of both holes and electrons is involved together with ionisation of underbonded oxide ions. In acceptor-doped, *p*-type materials, the possibility of a third mobile species associated with oxide ion (or oxygen vacancy) diffusion should not be ignored. Further studies are required to understand the factors that control the kinetics of the atmosphere- and bias-dependent conductivity changes seen here for BST materials. At this stage, we do not know whether there is a single rate-limiting process but suspect that there may be several, depending on conditions.

Conclusions

The solid solutions lose a small amount of oxygen, commencing at ~ 1400 °C in air. The mass changes were too small to be detected by thermogravimetry but were determined for one composition from mass changes in 0.5 g-sized pellets that had been either quenched or slow-cooled from 1470°C. Thus, the oxygen loss is reversible on slow cool but can be prevented by quenching.

Oxygen-deficient samples quenched from above 1400 °C are *n*-type; the conductivity increases greatly and the activation energy decreases with increasing oxygen deficiency. Slow-cooled samples are *p*-type and a modest increase in conductivity occurs with decreasing annealing temperature. There are numerous uncorrelated reports in the literature of both *n*- and *p*-type

behaviour in BT and it is presumed that there may also be a systematic dependence on annealing temperature, and a *p*- to *n*-type crossover, in BT similar to that reported here for BST.

The conductivity of *n*- and *p*-type BST solid solutions is sensitive to both pO_2 and *dc* bias, with, in part, similar mechanisms. In both cases, electrons are trapped at the sample surface in response to either increasing pO_2 or at the positive electrode on application of a *dc* bias. For *n*-type materials, the conductivity decreases as the concentration of mobile carriers decreases. For *p*-type materials, a second mechanism that takes place simultaneously involves the ionisation of underbonded oxide ions to form electron-hole pairs; the electrons diffuse to the surface where they are trapped; the holes that are generated remain on oxygen and become the dominant mobile species. Both hole creation and the trapping of electrons at sample surfaces, are reversed on returning to the original conditions.

The location of holes on oxygen is equivalent to the formation of O^- ions. While O^- ions are not usually considered as taking any significant part in oxide structures and their electrical properties, the occurrence of O^- ions can be rationalised by (i) the instability of O^{2-} ions in the gas phase and (ii) consideration of the conditions under which O^{2-} ions in the solid state may readily ionise.

The response of both *n*- and *p*-type BST to a *dc* bias may be likened to the charge and self-discharge of a leaky capacitor. *n*-type BST becomes less leaky as the capacitor is charged whereas *p*-type BST becomes more leaky. Similar capacitive effects occur as a consequence of changing pO_2 in the atmosphere surrounding the sample and indicate that small departures from local electroneutrality occur in ceramic oxides. These studies also show how the bulk electrical properties of materials may be modified by changes occurring at sample surfaces.

Supporting Information.

T_c , T_o vs x ; Lattice parameters and cell volume of the BST solid solution; and $\tan \delta$ as a function of temperature.

List of Figures.

Fig. 1. (a) Permittivity as a function of temperature at 100 kHz for a range of compositions sintered

at 1400 °C, (b) the corresponding Curie-Weiss plots

Fig. 2. (a,b) Impedance complex plane plots, Z^* , at two temperatures for $x = 0.2$; (c) spectroscopic plots of capacitance at different temperatures.

Fig. 3. Arrhenius plots (a) of R_1 and R_2 for $x = 0.2$ with Pt, Au and Ag electrodes and (b) R_1 for compositions, $x = 0.2, 0.3, 0.4, 0.5$ and 1.

Fig. 4. Impedance data for $x = 0.2$ in different atmospheres (a) at 550 °C for a sample slow-cooled from 1400 °C, (b) at 206 °C for a sample quenched from 1440 °C.

Fig. 5(a,b) Impedance data at 400 °C for $x = 0.2$ before and after 10 V was applied at different times; spectroscopic plots of (c) Y' and (d) C' at different times.

Fig. 6. Bulk conductivity of slow-cooled $x=0.2$ at 600 °C as a function of time with bias voltages of 1, 5 and 10 V (sample thickness 1.36 mm) in N_2 , air, and O_2 .

Fig. 7. Impedance data for $x = 0.2$ quenched from 1440 °C as a function of time with 10 V bias at 197 °C in air.

Fig. 8. Arrhenius plots of (a) R_1 for $x=0.2$: slow-cooled from 1400 °C and quenched from 1200, 1400, 1430, 1440, 1450 and 1470 °C, (b) R_1 for $x = 0.5$: slow-cooled from 1400 °C and quenched from 1400, 1430, 1450 and 1470 °C.

References

¹ M. McQuarrie, "Structural Behavior in the System (Ba,Ca,Sr)TiO₃ and Its Relation to Certain

- Dielectric Characteristics”, *J. Am. Ceram. Soc.* **1955** 444–449.
- ² J. A. Basmajian, and R. C. DeVries, “Phase Equilibria in the System BaTiO₃-SrTiO₃”, *J. Am. Ceram. Soc.* **1957** 373–376.
- ³ E. N. Bunting, G. R. Shelton, and A. S. Creamer, “Properties of Barium-Strontium Titanate Dielectrics”, *J. Res. Nat. Bur. Stand.* **1947** 337–349.
- ⁴ S. Kisaka, S. Ikegami, and H. Sasaki, “Dielectric Properties of Mixed Crystals of Barium-Strontium Titanate”, *J. Phys. Soc. Jpn.* **1959** 1680–1685.
- ⁵ B. Jaffe, W. R. Cook Jr and H. Jaffe, in *Piezoelectric Ceramics*, ed. J. P. Roberts and P. Popper, Academic Press, London, 1971, ch. 3, pp. 53–114.
- ⁶ H. Beltrán, M. Prades, N. Masó, E. Cordoncillo, and A. R. West, “Voltage-Dependent Low-Field Bulk Resistivity in BaTiO₃:Zn Ceramics”, *J. Am. Ceram. Soc.* **2010** 500–505.
- ⁷ M. Prades, N. Masó, H. Beltrán, E. Cordoncillo, and A. R. West, “Field enhanced bulk conductivity of BaTiO₃:Mg ceramics”, *J. Mater. Chem.* **2010** 5335–5344.
- ⁸ N. Masó, M. Prades, H. Beltrán, E. Cordoncillo, D. C. Sinclair, and A. R. West, “Field enhanced bulk conductivity of acceptor-doped BaTi_{1-x}Ca_xO_{3-x} ceramics”, *Appl. Phys. Lett.* **2010** 062907 3pp.
- ⁹ Q.-L. Zhang, N. Masó, Y. Liu, H. Yang, and A. R. West, “Voltage-dependent low-field resistivity of CaTiO₃:Zn ceramics”, *J. Mater. Chem.* **2011** 12894–12900.
- ¹⁰ H. Beltrán, M. Prades, N. Masó, E. Cordoncillo, and A. R. West, “Enhanced Conductivity and Nonlinear Voltage–Current Characteristics of Nonstoichiometric BaTiO₃ Ceramics”, *J. Am. Ceram. Soc.* **2011** 2951–2962.
- ¹¹ L. Gil Escrig, M. Prades, H. Beltrán, E. Cordoncillo, N. Masó, and A. R. West, “Voltage-Dependent Bulk Resistivity of SrTiO₃:Mg Ceramics”, *J. Am. Ceram. Soc.* **2014** 2815–2824.

- ¹² Y. Liu and A. R. West, “Voltage-Dependent Resistance of Undoped Rutile, TiO₂, Ceramics”, *Appl. Phys. Lett.* **2013** 263508 3pp.
- ¹³ M. Prades, H. Beltrán, E. Cordoncillo, P. J. Alonso, N. Masó, and A. R. West, “Non-ohmic phenomena in Mn-doped BaTiO₃”, *Phys. Status Solidi A* **2012** 2267–2272.
- ¹⁴ N. Masó, H. Beltrán, M. Prades, E. Cordoncillo, and A. R. West, “Field-enhanced bulk conductivity and resistive-switching in Ca-doped BiFeO₃ ceramics”, *Phys. Chem. Chem. Phys.* **2014** 19408–19416.
- ¹⁵ N. Masó, and A. R. West, “Electronic Conductivity in Ytria-Stabilized Zirconia under a Small *dc* Bias”, *Chem. Mater.* **2015** 1552–1558.
- ¹⁶ R. Moos and K. H. Härdtl, “Defect Chemistry of Donor-Doped and Undoped Strontium Titanate Ceramics between 1000° and 1400°C”, *J. Am. Ceram. Soc.* **1997** 2549–2562.
- ¹⁷ H. Beltrán, E. Cordoncillo, P. Escribano, D. C. Sinclair and A. R. West, “Oxygen loss, semiconductivity, and positive temperature coefficient of resistance behavior in undoped cation-stoichiometric BaTiO₃ ceramics”, *J. Appl. Phys.* **2005** 094102.
- ¹⁸ Y. Liu and A. R. West, “Semiconductor-Insulator Transition in Undoped Rutile, TiO₂, Ceramics”, *J. Am. Ceram. Soc.*, **2013** 218–222.
- ¹⁹ I. A. Alagdal and A. R. West, “Oxygen non-stoichiometry, conductivity and gas sensor response of SnO₂ pellets”, *J. Mater. Chem. A* **2015** 23213–23219.
- ²⁰ P. Ren, N. Masó, and A. R. West, “Hole conductivity in oxygen-excess BaTi_{1-x}Ca_xO_{3-x+δ}”, *Phys. Chem. Chem. Phys.* **2013** 20943–20950.

Table Captions.

Table 1. The weight of samples, $x = 0.2$, quenched and slow-cooled from 1470 °C; the oxygen

stoichiometry was calculated to be $\text{Ba}_{0.8}\text{Sr}_{0.2}\text{TiO}_{2.9885}$ at 1470 °C.

Table 1. The weight of samples, $x = 0.2$, quenched and slow-cooled from 1470 °C; the oxygen stoichiometry was calculated to be $\text{Ba}_{0.8}\text{Sr}_{0.2}\text{TiO}_{2.9885}$ at 1470 °C.

<i>sample</i>	<i>m (g)</i>
1470 °C slow cooled	0.4835
1470 °C quenched	0.4830
1470 °C slow cooled	0.4833
1470 °C quenched	0.4829
1470 °C slow cooled	0.4832
1470 °C quenched	0.4828

Figure Captions.

Fig. 1. (a) Permittivity as a function of temperature at 100 kHz for a range of compositions sintered

at 1400 °C, (b) the corresponding Curie-Weiss plots

Fig. 2. (a,b) Impedance complex plane plots, Z^* , at two temperatures for $x = 0.2$; (c) spectroscopic plots of capacitance at different temperatures.

Fig. 3. Arrhenius plots (a) of R_1 and R_2 for $x = 0.2$ with Pt, Au and Ag electrodes and (b) R_1 for compositions, $x = 0.2, 0.3, 0.4, 0.5$ and 1.

Fig. 4. Impedance data for $x = 0.2$ in different atmospheres (a) at 550 °C for a sample slow-cooled from 1400 °C, (b) at 206 °C for a sample quenched from 1440 °C.

Fig. 5(a,b) Impedance data at 400 °C for $x = 0.2$ before and after 10 V was applied at different times; spectroscopic plots of (c) Y' and (d) C' at different times.

Fig. 6. Bulk conductivity of slow-cooled $x=0.2$ at 600 °C as a function of time with bias voltages of 1, 5 and 10 V (sample thickness 1.36 mm) in N_2 , air, and O_2 .

Fig. 7. Impedance data for $x = 0.2$ quenched from 1440 °C as a function of time with 10 V bias at 197 °C in air.

Fig. 8. Arrhenius plots of (a) R_1 for $x=0.2$: slow-cooled from 1400 °C and quenched from 1200, 1400, 1430, 1440, 1450 and 1470 °C, (b) R_1 for $x = 0.5$: slow-cooled from 1400 °C and quenched from 1400, 1430, 1450 and 1470 °C.

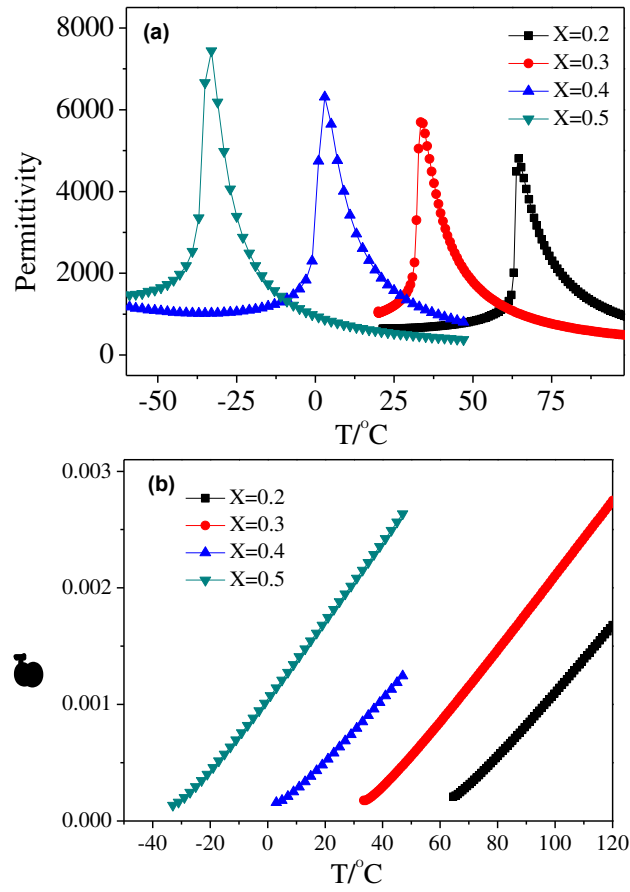


Fig. 1. (a) Permittivity as a function of temperature at 100 kHz for a range of compositions sintered at 1400 °C, (b) the corresponding Curie-Weiss plots

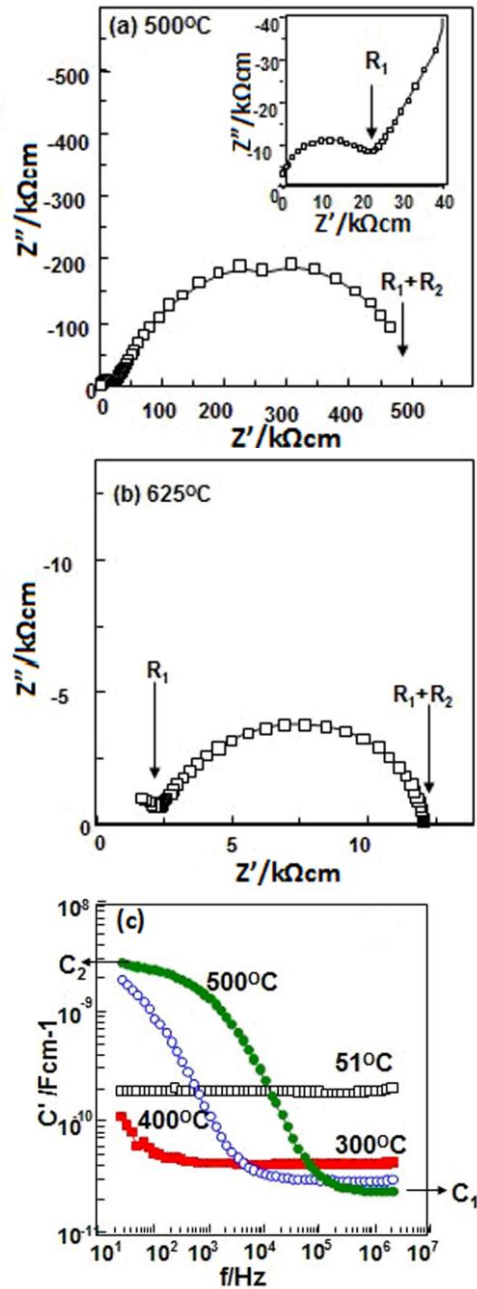


Fig. 2. (a,b) Impedance complex plane plots, Z^* , at two temperatures for $x = 0.2$; (c) spectroscopic plots of capacitance at different temperatures.

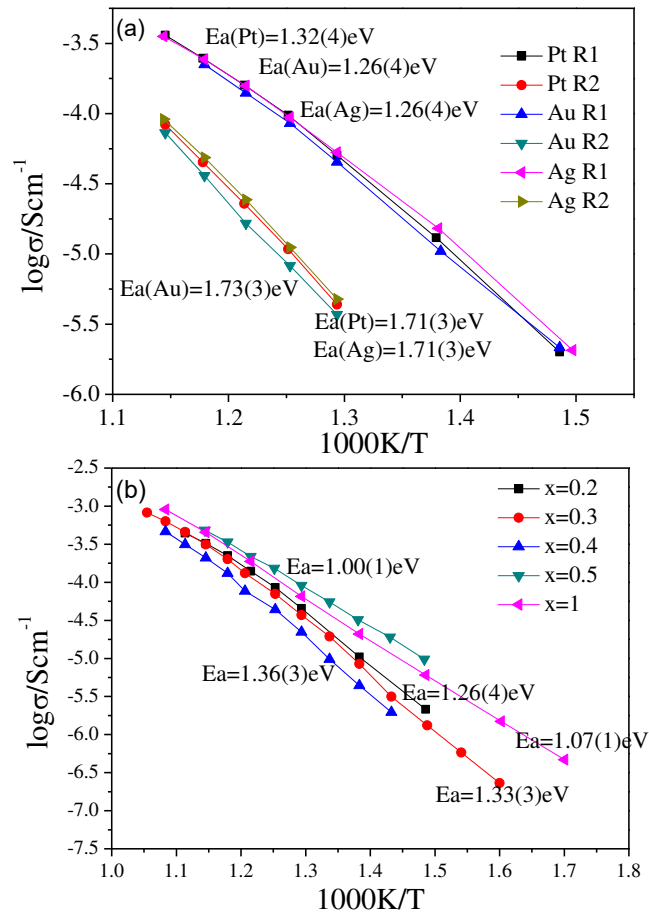


Fig. 3. Arrhenius plots (a) of R_1 and R_2 for $x = 0.2$ with Pt, Au and Ag electrodes and (b) R_1 for compositions, $x = 0.2, 0.3, 0.4, 0.5$ and 1 .

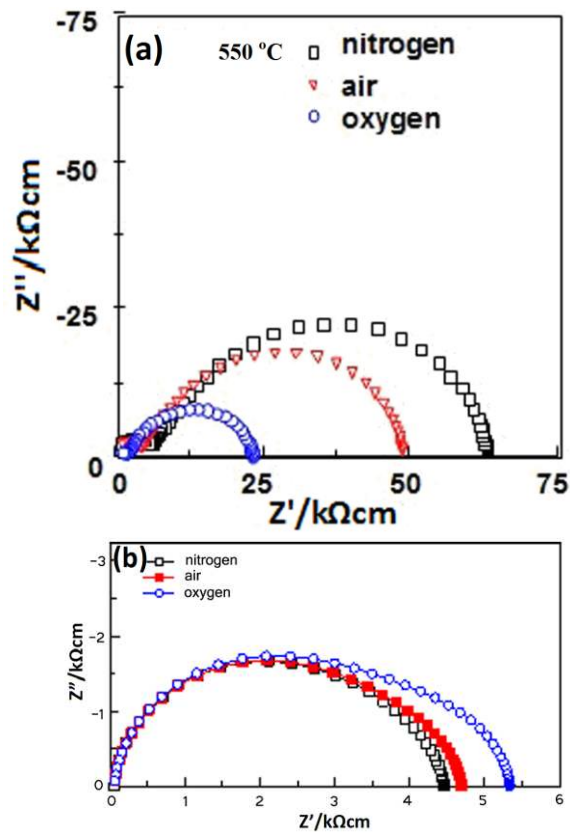


Fig. 4. Impedance data for $x = 0.2$ in different atmospheres (a) at 550 °C for a sample slow-cooled from 1400 °C, (b) at 206 °C for a sample quenched from 1440 °C.

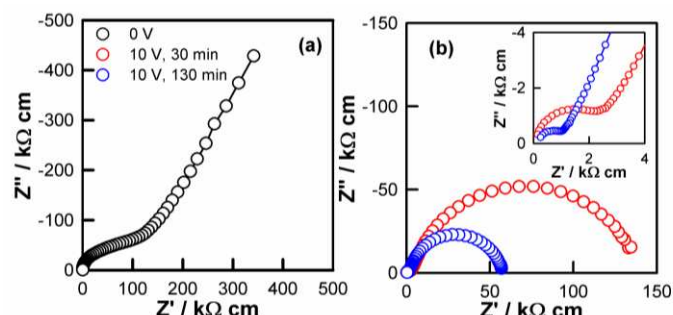


Fig. 5(a,b) Impedance data at 400 °C for $x = 0.2$ before and after 10 V was applied at different times; spectroscopic plots of (c) Y' and (d) C' at different times.

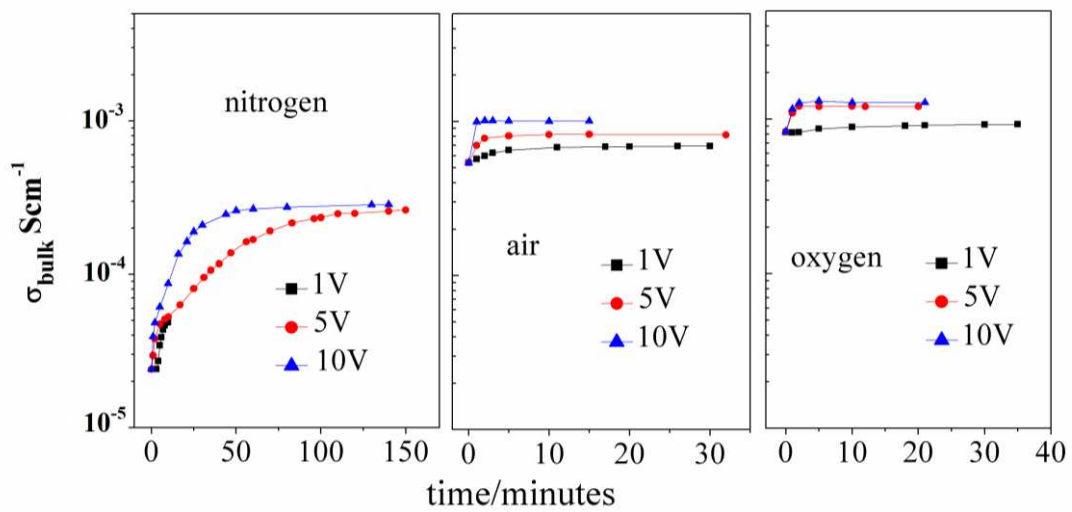


Fig. 6. Bulk conductivity of slow-cooled $x=0.2$ at 600 °C as a function of time with bias voltages of 1, 5 and 10 V (sample thickness 1.36 mm) in N_2 , air, and O_2 .

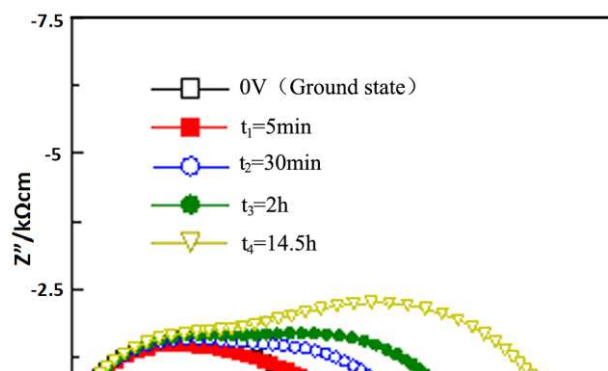


Fig. 7. Impedance data for $x = 0.2$ quenched from $1440\text{ }^\circ\text{C}$ as a function of time with 10 V bias at $197\text{ }^\circ\text{C}$ in air.

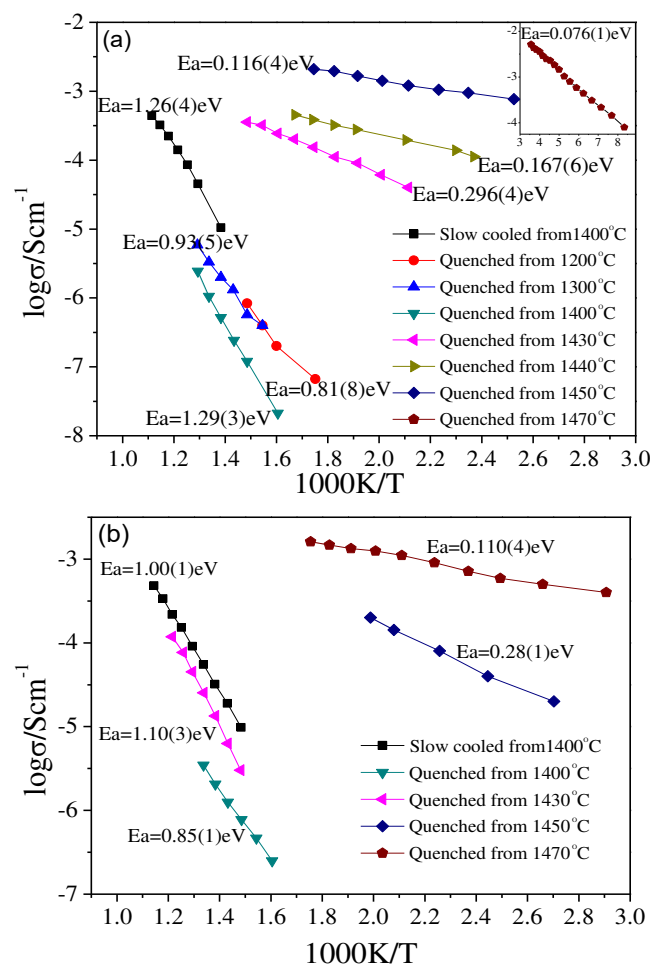
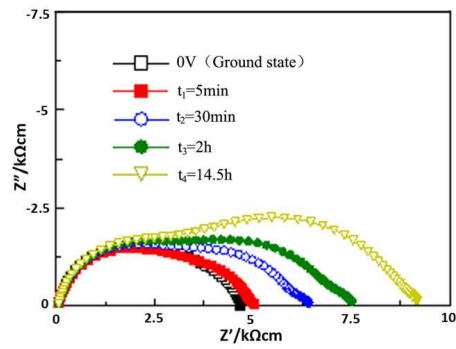


Fig. 8. Arrhenius plots of (a) R_1 for $x=0.2$: slow-cooled from $1400\text{ }^\circ\text{C}$ and quenched from 1200 , 1400 , 1430 , 1440 , 1450 and $1470\text{ }^\circ\text{C}$, (b) R_1 for $x = 0.5$: slow-cooled from $1400\text{ }^\circ\text{C}$ and quenched from 1400 , 1430 , 1450 and $1470\text{ }^\circ\text{C}$.

“For Table of Contents Only”



The conductivity of *n*-type materials decreased when a small *dc* bias is applied across the sample, whereas *p*-type show increased conductivity under the same conditions. The reduced *n*-type conductivity is attributed to trapping of mobile carriers at the positive electrode whereas the enhanced *p*-type conductivity is attributed to creation and location of mobile holes, on underbonded oxide ions, in the sample interior.